Since January 2020 Elsevier has created a COVID-19 resource centre with free information in English and Mandarin on the novel coronavirus COVID-19. The COVID-19 resource centre is hosted on Elsevier Connect, the company's public news and information website.

Journal of the Indian Chemical Society 98 (2021) 100272

Contents lists available at ScienceDirect

Journal of the Indian Chemical Society

journal homepage: www.editorialmanager.com/JINCS/default.aspx

In silico validation of anti-viral drugs obtained from marine sources as a potential target against SARS-CoV-2 M^{pro}

Srijit Ghosh [a,*,1], Srijita Das [a,1], Iqrar Ahmad [b], Harun Patel [b]

[a] Guru Nanak Institute of Pharmaceutical Science and Technology, Sodepur, Kolkata, 700114, West Bengal, India
[b] Department of Pharmaceutical Chemistry, R. C. Patel Institute of Pharmaceutical Education and Research, Shirpur, Maharashtra, 425405, India

ARTICLE INFO

Keywords:
COVID-19
Marine
MD simulation
Pharmacokinetics
Viral main protease

ABSTRACT

COVID-19 caused by Severe Acute Respiratory Syndrome Coronavirus-2 (SARS-CoV-2) has threatened the whole world affecting almost 243 million people globally. Originating from China, it has now spread worldwide with USA and India being the two most affected countries which emphasizes the immense potential of the coronaviruses to cause severity in the human population. This study validates the efficacy of some marine antiviral agents to target the viral main protease (Mpro) of SARS-CoV-2 by in silico studies. A total of 14 marine-derived antiviral agents were screened from several databases including PubChem and DrugBank and docked against the crystallised 3D structure of SARS-CoV-2 Mpro. MD simulation of the top two ligands was carried out for 100 ns to validate the protein-ligand stability. Later, their physicochemical, pharmacokinetics, and drug-likeness properties were evaluated and toxicity prediction was performed using eMOLTOX webtool. We found that all the 14 compounds are acting as a good target for Mpro. Among them, avarol and AcDa-1 procured the best docking results with the estimated docking score of −8.05 and −7.74 kcal/mol respectively. MD simulation revealed good conformational stability. The docked conformation was visualised and subsequent ligand-amino acid interactions were analysed. Avarol revealed good pharmacokinetic properties with oral bioavailability. The overall finding suggested that these marine compounds may have the potential to be used for the treatment of COVID-19 to tackle this pandemic.

1. Introduction

COVID-19 has conquered almost every part of the world, first identified in December 2019 from the famous fish market of Wuhan in China and the probable reason for its transmission is via zoonotic medium [1]. The real culprit behind this disease was found to be a relatively bigger group of RNA viruses belonging to the β-coronavirus genus and was named 2019-nCoV or SARS-CoV-2 due to its genetic similarity to the SARS-CoV virus. Within 3 months, it conquered the world due to its rapid transmission rate among people, and that is the reason it resulted in a worldwide pandemic still being faced globally [1,2]. In India, the 1st case of COVID-19 was recorded on 30 January 2020 from Thrissur district of Kerala, and now the count has risen to almost 110 million confirmed cases in October 2020. Recently, cases of COVID-19 were also seen in isolated remote tribes of Andaman island, India. The majority of the COVID-19 cases recorded are mild and many are asymptomatic with prominent symptoms of pneumonia and acute respiratory distress syndrome (ARDS) [3]. Around 30,000 nucleotides are present in the virus which encodes for numerous structural as well as non-structural proteins [4,5]. After gaining entry into the host cell, the virus releases its genomic material, incorporates it with the host genome, and translates to form poly-peptides (pp1a and pp1b). These poly-peptides are broken down into many functionally active small proteins by viral main protease (Mpro/3CLpro) which are required for viral replication. Hence, Mpro serves as an important agent for viral survival and growth and not many mutations have been observed in this enzyme [1,6]. This enables the researchers to target Mpro to essentially halt the viral transmission. Several drugs have been targeted to Mpro, including antivirals like Darunavir, Saquinavir but their efficacy still remains questionable. According to computational studies, an antipsychotic drug, Lurasidone, and antibiotic, Talampicillin possess the highest binding affinity towards Mpro [7,8].

Researchers are investigating natural compounds to find a better target for Mpro as synthetic derivatives are prevailing good results, but

* Corresponding author.
E-mail address: srijitgh@gmail.com (S. Ghosh).
[1] Authors with equal contributions.

https://doi.org/10.1016/j.jics.2021.100272
Received 17 February 2021; Received in revised form 27 October 2021; Accepted 17 November 2021

simultaneously showing increased side-effects, toxicity, long course of treatments that are restricting their effectiveness. With intense findings on the ground is still going on, now the researchers are aiming towards the marine sources in the hope to find a better target. The earth is surrounded by almost 70% water which consists of almost 90% of biodiversity. The significant exploration of the marine ecosystem started just around 50 years ago which created a massive development in pharmaceuticals. Uncountable numbers of anti-viral agents have been isolated from marine sources over the past 30 years. In the search for an effective and safe marine agent to combat SARS-CoV-2, we have chosen 14 marine antivirals and docked them against the main protease (Mpro) of the virus to check their inhibitory activities [9].

1.1. SARS-CoV-2: coronavirus that caused pandemic

Currently, the whole world is undergoing a serious pandemic due to the transmission of a β-group of coronavirus named Severe Acute Respiratory Syndrome coronavirus-2 (SARS-CoV-2) causing the disease COVID-19 [1]. It is a zoonotic type of infection that was seen to jump from animal carriers to humans [10]. In December 2019, the first occurrence of COVID-19 was seen in a fish supermarket in Wuhan, China as virus samples were first identified from that place. The SARS-CoV epidemic (2003) was seen to transmit from civet cats and bats while the MERS-CoV outbreak (2012) was transmitted from *Camelus dromedarius* camel to humans, but the exact carrier of SARS-CoV-2 is still unknown [2,3,11]. Many kinds of research claim to transmit from bats, which moved to other animals and at last end in humans, while others believe it to transmit from pangolins [12]. One research showed that snakes are also likely to be a prominent carrier of the virus. It is (+)-sensed single-stranded, non-segmented, enveloped RNA virus with 26–32 kb size [2]. Comparing SARS and MERS, SARS-CoV-2 is milder but the major drawback is its very high community transmission rate. The transmission rate is estimated by noting the basic reproduction number (R_0) which was found to be 2.6, which means one infected person can transmit the virus to 1.4 to 3.8 healthy persons with a mortality rate of around 2%. The virus can spread even from an asymptomatic patient which creates an extra burden in its high transmission rate [13,14]. The mortality rate is highest in the people of the age of 75 years and above (48.7%), while children between the age of 0–17 years old are the least affected (0.06%). A study was conducted by New York City Health in April 2020 regarding the mortality ratio between males and females and it was found that around 61.8% of males and 38.2% of females were deceased due to the virus. Comorbidities impart another serious factor in this disease. People with pre-existing disorders like cardiovascular disease, hypertension, diabetes, chronic respiratory disease, or cancer have a greater risk of comorbidities if infected by COVID-19 (0.9%) [15,16]. The latest total cases of COVID-19 recorded as per WHO on December 23, 2021 were 243,851,805 with a recovery of 220,946,756 and deaths 4, 955,454. India currently has the second-highest active COVID-19 cases (34,174,887) preceding the USA. The symptoms of COVID-19 begin to appear after an incubation period of 2–14 days, but Hubei Province's local government reported some cases with 27 days of the incubation period. Initial symptoms include fever with chills, sore throat, dry cough, shortness of breath, accompanied by pain in muscles, headache, skin rashes, diarrhoea, fatigue with loss of taste sensation, but 80% of cases are mild. According to WHO, out of 5 patients, at least 1 requires to be admitted to the hospital [17].

1.1.1. Replication cycle of SARS-CoV-2

The virus imparts a unique replication technique. It has a crown-like spike protein (S) of 150 kDa weight embedded on the outer surface of the virion. The S protein acts as the main element which conjugates with host cell Angiotensin-Converting Enzyme (ACE-2) and Transmembrane Protease, Serine 2 (TMPRSS2) receptor and enters the host cell. Other structural proteins of the virus include envelope (E), nucleocapsid (N), transmembrane glycoprotein (M), and other adjunct proteins [18,19]. M protein has a molecular weight of around 25–30 kDa which provides the shape of the virion. N protein is a highly phosphorylated protein and forms the capsid. E protein is having a molecular weight of 8–12 kDa that forms the envelope and helps in the assembly and exit of the virion from the host cell [20,21]. The virus is transmitted via respiratory droplets, saliva and secretions shed by an infected person and enter into a healthy person by direct contact to nose, mouth, or eyes. After entering the host body, it rapidly multiplicates at the lower region of the ciliary epithelium of the airway tract. There it attaches the host cell receptor via S protein homodimer formation. S protein has two subunits- S1 and S2. S1 subunit binds with ACE-2 receptor. S2 subunit contains fusion proteins that are cleaved and thus activated by host cell transmembrane protease, serine 2 (TMPRSS2) or pH-dependent cysteine protease, cathepsin-L thus allowing the entry of the virus into the host cell cytoplasm via endosome formation. Uncoating occurs which causes the release of viral RNA [22,23]. The viral mRNA is supplemented by around 14 open reading frames (ORFs) coding for several non-structural and structural proteins of the virus. Two sub-domains, ORF1a and ORF1b undergo translation and forms pp1a and pp1ab polyproteins. pp1a is further cleaved by chymotrypsin-like protease (3CLpro or Mpro) and papain-like proteases (PLpro) enzymes to form non-structural protein, nsps 1–11, and similarly, pp1ab cleaved to form nsps 1–16. Among them, nsp 12 plays the function of RNA-dependent RNA polymerase (RNA replicase) which assists in transcribing to an intermediate (−)-sense viral genomic RNA that is later transcribed again to (+)-sense RNA. On the other hand, the mRNA is translated at the endoplasmic reticulum-bound ribosome to form N, E, M, S structural proteins. Later, these proteins are embedded in the ER, transferred to the endoplasmic reticulum-Golgi intermediate compartment (ERGIC) and the viral genomic RNA meets with each other and all together they form small unit vesicles and become ready to release from the host cell [20,24,25].

1.1.2. Inhibiting viral main protease enzyme

The virus forms two known proteases: papain-like proteases (PLpro), chymotrypsin-like protease (3CLpro). Among them, 3CLpro is considered the main protease and is also known as Mpro [26]. It is encoded by nsp5 protein which is formed by the auto-cleavage of pp1ab protein. It is formed from 306 amino acids and differs from the main protease of SARS-CoV in just 12 amino acids. It cleaves the other polyprotein at Leu Gln↓ (Ser, Ala, Gly) (↓ denotes the site of cleavage) site by forming a dimer. Protease plays a major part in the formation of active proteins (proteome) crucial for viral replication. Hence, inhibiting protease can yield a better target to limit COVID-19 replication [19,26]. HIV protease inhibitors like lopinavir, ritonavir, darunavir are currently undergoing clinical trials to check their efficacy against 3CLpro enzyme of COVID-19, but one clinical trial by *Jansenn Pharmaceutica* claimed that the combinational usage of cobicistat along with darunavir didn't show better results against the SARS-CoV-2 virus [27]. Similarly, Hepatitis-C Virus (HCV) protease inhibitors such as velpatasvir and ledipasvir were also seen to impede 3-CLpro/Mpro by *in-silico* studies [28]. Teli D.M. et al. studied a wide range of compounds including coumarins, terpenoids, glycosides, flavonoids, phenols and polyphenols, catechins. Flavonol glycosides such as quercitrin, rutin, baicalin, astragalin, myricetin-3-glucoside, and amentoflavone exhibited superior docking scores than the other categories of flavonoids investigated, whereas MPro binding affinity was modest for daidzein and genistein [29]. Ibrahim et al. suggested that DB02388 and Cobicistat might be useful as SARS-CoV-2 Mpro inhibitors [30]. Certain antibacterials like doxycycline, demeclocycline, and lymecycline; antihypertensive drugs like telmisartan and nicardipine, and even leukotriene inhibitors such as montelukast have shown a prominent affinity towards Mpro in computer modelling [31].

1.2. Marine anti-virals having potential to target SARS-CoV-2

The earth is almost surrounded by 1/3rd of oceans and sea.

Uncountable marine habitats exist in which the majority is still unexplored. It is necessary to tap the marine fauna and flora for the commercial utility of novel drugs which can be used for the treatment of several incurable disorders. Although the use of marine plants and animals is done for food purposes, but we still lack in exploring the real benefits which we can get from the oceans, and so, serious consideration of these organisms as sources of biologically active compounds has been confirmed in the last 40 years. Certain well-known products from marine sources are currently being utilised like halibut and cod liver oil obtained from *Hippoglossus vulgaris* and Atlantic cod fish (*Gadus morhua*) respectively which serve as a rich source of vitamin A and D [32]. Protamine sulphate is extracted from sperms of salmon fish serves as an antidote for heparin toxicity. Other products like spermaceti, carrageenan, alginic acid, agar, and seaweed polysaccharides have a wide range of pharmaceutical uses. Many seaweeds are extensively used as multivitamins in controlling anaemia during pregnancy or in the treatment of hypothyroidism, anti-diabetics, vermifuges, and many more. Out of all the uses, researchers have obtained numerous potent antiviral agents with extraordinary activities against several serious pathogenic viruses like HIV, HSV1/2, dengue virus, Human Cytomegalovirus (HCMV), and influenza.

Fucoidan is a sulphated polysaccharide composed of sulphate groups linked with L-fucose. It is mainly isolated from different species of brown seaweed algae which include bladderwrack, kombu, wakame, hijiki, and mozuku. It is also found in the sea cucumber. Apart from antiviral activity, it shows numerous other therapeutic uses including anticoagulant, anticancer, immunomodulatory, and neuroprotective actions. Clinical research has also seen it to lower high blood pressure and reduce inflammation. Although its mechanism of action is not clear, its antiviral activity is supposed due to the downregulation of Type 1 Insulin-Like Growth Factor (IGF-1R), and Activator Protein-1 (AP-1) signalling pathways and stimulation of NK cells [33–35].

Chondroitin sulphate is composed of sulphated glycosaminoglycan (GAG) which consists of alternating sugars like glucuronic acid and N-acetyl galactosamine (NAG). It is obtained from marine animals such as sharks. It is widely used for the treatment of osteoarthritis, breast cancer, hypercholesterolemia, Gastroesophageal Reflux Disease (GERD), soreness of muscles, and bone joint pain. It also has a very prominent antiviral activity and is used in the management of HIV/AIDS. Sano Y. examined the inhibition of Tobacco Mosaic Virus (TMV) infection by chondroitin sulphate. Kato D. et al. found that chondroitin sulphate can effectively stop the replication of the dengue virus by blocking Dengue Virus (DENV) E-protein [36].

Iota-Carrageenans belong to a family of sulphated polysaccharides that are isolated by alkaline extraction of red edible seaweeds. They are mostly find used in the food industry because of their gelling, thickening, and stabilizing properties. The antiviral action of iota-carrageenan was first found in mumps and influenza-B virus by Gerber P. et al. Later with the advancement of researches, its broad-spectral antiviral action was found eminent against HSV, papillomavirus, dengue virus, HAV, and HCMV. The negative charge of iota-carrageenan assists in trapping the surface of the airway virus and thus prevents viral replication [37,38].

Fostularin 3 is a cytotoxic molecule that binds via hydrophobic and hydrogen bond formation with the active residues of Mpro of SARS-CoV-2.

1-Hexadecoxypropane-1,2-diol and 15 alpha-methoxypuupehenol also find an affinity towards Mpro inhibiting it. 1-hexadecoxypropane-1,2-diol consists of a long lipophilic chain that interacts with the hydrophobic moiety of the protein. Nasu S. S. et al. reported moderate antiviral activity of 15 alpha-methoxypuupehenol [39].

Vidarabine, also known as Ara-A sourced from a marine sponge named *Tethya crypta*, imparts potent antiviral activity, especially against varicella-zoster virus, HSV, and some RNA viruses. It is a nucleoside analog that acts by interfering with viral DNA synthesis. Its capability to bind with Mpro of SARS-CoV-2 is also being established [40].

Phycocyanobilin is a phytochrome chromophore procured from the algae of Arthrospira sp. It shows a wide range of antiviral actions by acting against HSV, HCV, influenza, HIV, etc. Phycocyanobilin and other Arthrospira species act by blocking EV71 RNA synthesis and forming viral plaque, thus inhibiting viral growth [41].

Avarol is derived from the marine sponge *Disidea avara*. It is sesquiterpene hydroquinone in nature. It is active against HIV AIDS, HTLV-III. It inhibits GAG proteins p24 and p17 which form viral capsid and viral tegument [42].

Macrolactin-A chemically represents 24-membered lactones exerting powerful antiviral and antibacterial activities. The mode of action of macrolactin-A is probably due to phosphatase inhibitory action. Potent in vitro inhibitory action against Herpes simplex virus and HIV has been explored [43].

AcDA-1 is obtained from the marine algae *Dictyota menstrualis*. Pereira H. S. et al. demonstrated the anti-retroviral activity of AcDA-1 by checking the viral load in the PM-1 cell at different time intervals after administration of the drug. The results were promising as the drug was able to inhibit the virus at its early stage of replication. The reason for the antiviral activity is due to the dose-dependent inhibition of reverse transcriptase of HIV [44].

Esculetin-4-carboxylic acid ethyl ester is a coumarin derivative that is extracted from another species of marine sponge named *Axinella* cf. *corrugate*. Lira S. et al. in 2007 demonstrated the in vitro activity of esculetin-4-carboxylic acid ethyl ester by inhibiting 3CLpro of SARS. A similar experiment was performed by Hamill P. et al. to identify the novel anti-SARS agent from *Axinella corrugate*. Hence, it may also inhibit 3CLpro of SARS-CoV-2 due to the structural similarity of protease enzyme in both of the viruses [45,46].

Hydroxypentafuhalol A is obtained from a variety of brown seaweed algae named *Sargassum spinuligerium*. The antiviral activity is mainly achieved due to the polysaccharides present in them. Other uses include anticancer, antioxidant, and antimicrobial activity [47].

6,6′-Bieckol is a phloroglucinol derivative extracted from brown algae *Ecklonia cava*. Artan M. et al. observed potent anti-HIV activity of 6,6′-bieckol by directly inhibiting HIV-1 reverse transcriptase enzyme without causing any cytotoxicity to the host cells. Other probable mechanism includes blocking viral p24 and imparts lytic actions to halt the viral reproduction [48]. A type of phlorotannin extracted from *Ecklonia kurome* and *Eisenia bicyclis* is 8,8′-bieckol which is a structural isomer of 6,6′-bieckol. Antiviral activity against HPV was observed by Kim E. B. et al. after evaluating the sample on HPV18PV and HPV16PV infected 293 TT cells via bio-luminescence (SEAP) assay method [49].

2. Materials and methods

2.1. Ligand selection

A total of 14 clinically approved compounds from marine sources were screened from numerous ligands which yield potent anti-viral activity. The structures and information of all the compounds were taken from PubChem (https://pubchem.ncbi.nlm.nih.gov/) and DrugBank database (https://www.drugbank.ca/) [50,51]. The canonical SMILES were collected and 3D interpretation was done from Corina Classic (https://www.mn-am.com/online_demos/corina_demo) webtool.

2.2. Macromolecule selection

The 3D crystal structure of SARS-CoV-2 main protease, Mpro was selected from RCSB PDB [52]. The protein with PDB code 7D1M was selected for the task where Mpro was bound with GC376. The protein structure inhibitors were separated by releasing the atomic coordinates, using UCSF Chimera to get Mpro protein in the free form [53]. AutoDock Tools version 1.5.6 was used to add all the missing hydrogens, designation of partial charges, calculating Gasteiger charges to the macromolecule.

2.3. Protein grid box generation

A grid box is a method of allotment of a particular 3D area in the protein where the ligand will bind with the appropriate pockets in the receptor to impart activity. At AutoDock 4.2.6, the grid box was adjusted before docking to make the ligand in a flexible form when interacting with macromolecules under rigid conditions [54]. After extracting the.PDB files of the ligand and protein, all the water molecules were removed from the protein, and polar hydrogens were added. The suitable binding area was adjusted around the active binding site of the protein using AutoDock 4.2.6 where the ligand can search for better binding with minimum energy by allotting x, y and z-axis with suitable spacing. In case of Mpro, we designated the grid box of dimensions: x axis = 40 Å, y axis = 40 Å, z axis = 40 Å with spacing of 0.353 Å. The grid box was centred on X centre: 7.217 Å, y centre: 2.206 Å and z centre: 22.36 Å.

2.4. Molecular docking

After adjusting the receptor grid box, the next task was to make the molecule ready for docking. This task was also performed at AutoDock 4.2.6. The lowest docking score was taken as the final ΔG values and the predicted IC_{50} (K_i) values were recorded. After docking, the conformation at the hydrophobic surface and protein-ligand interactions were studied at PMV-1.5.6 [55]. and Pymol [56] to confirm their antagonistic actions.

2.5. MD simulation study

Molecular dynamics (MD) simulations for the top two docked protein-ligand complex were carried out using the Schrödinger Desmond program, an explicit solvent MD package along with a fixed OPLS 2005 force field [57]. The protein-ligand complex was prepared in protein preparation wizard with the predefined SPC (simple point charge) water model and orthorhombic box shape (size of the box as 10 Å × 10 Å × 10 Å distance). The sodium chloride with the approximately physiological concentration of 0.15 M was placed in 10 Å buffer regions between the protein atoms and simulation box to set the ionic strength using the system-built option. Minimisation jobs were performed to relax the system into a local energy minimisation, afterwards this model system was submitted to 100ns MD simulation steps using with OPLS_2005 force field. Noose-Hover chain thermostat algorithm at 300 K, Martyna-Tobias-Klein barostat algorithm at 1.01325 bar, isotropic coupling, Coulombic cut off at 0.9 nm. The rest of the parameters were default [58,59]. The trajectories of MD simulations evaluated for ligand-receptor interactions were identified using the Simulation Interaction Diagram (SID) tool.

2.6. ADME analysis

After obtaining an acceptable docking score, the pharmacokinetic specifications, physicochemical and drug-likeness properties of the ligand were examined using SwissADME (http://www.swissadme.ch/) and ADMETlab (http://admet.scbdd.com/#) servers [60,61].

2.7. Toxicity prediction

Finally, the toxicity prediction was performed at eMOLTOX webtool where probable toxicities were recorded by analysing different moieties present in the drug. This can briefly state whether the drug is safe for human consumption despite good therapeutic activity [62].

3. Result and discussion

3.1. Enumeration of the marine drugs used

A total of 14 clinically approved marine drugs were selected from PubChem for analysis (Table 1) [50]. All the selected drugs had been seen to exert some sort of anti-viral activity. Hence, the action of those drugs is required to be checked on the main protease (Mpro) of SARS-CoV-2. Fourteen drugs include fucoidan, chondroitin sulphate, iota-carrageenan, fostularin 3, 1-hexadecoxypropane-1,2-diol, 15 alpha-methoxypuupehenol, Ara- A (vidarabine), phycocyanobilin, avarol, macrolactin-A, AcDa-1, esculetin-4-carboxylic acid ethyl ester, hydroxypentafuhalol A, and 6,6′-bieckol. The origin of most of the drugs is from Plantae sources like algae, seaweeds, though Animalia also includes sponges, shark cartilages, etc. PUBCHEM CID along with their respective IUPAC nomenclatures and molecular formula has been depicted in the table below for better clarification about the compounds [50].

The 2D structures (Fig. 1) of the following compounds were collected from ACD/ChemSketch 14.0 [63], and it was merely converted to its 3D form with the help of 3D structure generator tools like CORINA Classic where the 3D structures can be obtained by uploading the respective SMILES of the compounds. The 3D structures were analysed at UCSF Chimera and AutoDock 4.2.6 [53,54]. The torsion root was then detected and the number of rotatable and non-rotatable bonds were predicted. Fucoidan had 5 rotatable bonds out of 32 bonds. Rotation of the bonds occurred at C3, C4, C5, S10, and O13 positions. Similarly, chondroitin sulphate had 13 bonds, iota-carrageenan had 22 bonds, fostularin 3 had 16 bonds, 1-hexadecoxypropane-1,2-diol had 19 bonds, 15 alpha-methoxypuupehenol had 3 bonds, Ara- A (vidarabine) had 6 bonds, phycocyanobilin had 14 bonds, Avarol had 4 bonds, macrolactin-A had 3 bonds, AcDa-1 had 8 bonds, esculetin-4-carboxylic acid ethyl ester had 5 bonds, hydroxypentafuhalol A had 22 bonds, and 6,6′-bieckol had 17 rotatable bonds.

3.2. The protein: Mpro

The main protease enzyme of SARS-CoV-2 forms dimer and cleaves pp1a and pp1ab polypeptides at Leu Gln↓ (Ser, Ala, Gly) site, thus converting into active non-structural proteins which are required in viral replication [64]. The 3D crystal structure of Mpro was extracted by X-ray crystallography with a resolution of 1.35 Å and it was again co-crystallised with GC376 as an inhibitor to yield the protein with PDB code 7D1M (Fig. 2) [52]. The protein has 2 subunits: A and B with an overall molecular mass of 68.81 kDa (determined by mass spectroscopy). The total number of a non-hydrogen atom includes 5636. The catalytic site was pre-determined at residue CYS145 and HIS41, and likewise, the grid-box was made so that the docking must occur at the active binding site of the Mpro. Hence, the active binding site of inhibition may vary from different ligands [65]. The water molecules present in the protein were removed and only free A subunit was used for docking purposes.

3.3. ADME analysis

After a successful docking study, the next target was to analyse the physicochemical and pharmacokinetic properties of the compounds. This task was done with the help of SWISS ADME and ADMETlab where in-depth details of all the properties were predicted from the structure of the ligands (Tables 2 and 3) [60,61]. Among the following ligands, chondroitin sulphate and iota-carrageenan had maximum water solubility whereas 6,6′-bieckol had poor water solubility due to highly lipophilic moieties present in their structure. Despite moderate solubility of 1-hexadecoxypropane-1,2-diol, 15 alpha-methoxypuupehenol, avarol, and AcDa-1, all of them could permeate the blood-brain-barrier and may enter the brain (Table 2). If we look towards drug-likeness, fucoidan, 1-hexadecoxypropane-1,2-diol, 15 alpha-methoxypuupehenol, ara- A, phycocyanobilin, avarol, macrolactin-A, AcDa-1, and esculetin-4-carboxylic acid ethyl ester obeys the Lipinski's rule of 5 (Pfizer's rule). This rule gives an idea if the compounds are orally active. It is based on 5 criteria: molecular weight of the ligand should be less than 500 Da; Not greater than 5H bond donors; Not more than 10H bond

Table 1
List of 14 clinically approved drugs used to check their properties in SARS-CoV-2 main protease. The PUBCHEM CID along with their molecular formula, IUPAC name and biological origin are given in the table for easy interpretation.

Sl. No.	COMPOUND	PUBCHEM CID	IUPAC NAME	ORIGIN/SOURCE
1.	Fucoidan	92023653	[(2S,3S,4S,5S,6R)-4,5-dihydroxy-2,6-dimethyloxan-3-yl] hydrogen sulphate	Brown algae, Sea cucumber
2.	Chondroitin sulphate	24766	(2S,3S,4S,5R,6R)-6-[(2R,3R,4R,5R,6R)-3-acetamido-2,5-dihydroxy-6-sulfooxyoxan-4-yl] oxy-3,4,5-trihydroxyoxane-2-carboxylic acid	Shark cartilage
3.	Iota-carrageenan	11966245	[(2R,3R,4R,5R,6S)-4,5-dihydroxy-6-[[(1R,3R,4R,5S,8S)-3-[(2R,3S,4R,5R,6S)-5-hydroxy-2-(hydroxymethyl)-6-[[(1R,3S,4R,5S,8S)-3-hydroxy-4-sulfonatooxy-2,6-dioxabicyclo [3.2.1]octan-8-yl]oxy]-3-sulfonatooxyoxan-4-yl]oxy-4-sulfonatooxy-2,6-dioxabicyclo [3.2.1]octan-8-yl]oxy]-2-(hydroxymethyl)oxan-3-yl] sulphate	Sulphated polysaccharides obtained from marine red algae
4.	Fostularin 3	11170714	(5S,6R)-7,9-dibromo-N-[(2R)-3-[2,6-dibromo-4-[2-[[(5S,6R)-7,9-dibromo-6-hydroxy-8-methoxy-1-oxa-2-azaspiro[4.5]deca-2,7,9-triene-3-carbonyl]amino]-1-hydroxyethyl] phenoxy]-2-hydroxypropyl]-6-hydroxy-8-methoxy-1-oxa-2-azaspiro[4.5]deca-2,7,9-triene-3-carboxamide	Marine source
5.	1-Hexadecoxypropane-1,2-diol	21646261	1-hexadecoxypropane-1,2-diol	Marine source of Aplysinidae family
6.	15 alpha-Methoxypuupehenol	21591485	(4aS,6aS,12S,12aS,12bS)-12-methoxy-4,4,6a,12b-tetramethyl-1,2,3,4a,5,6,12,12a-octahydrobenzo[a]xanthene-9,10-diol	Marine sponge (Hyrtios species)
7.	Ara- A (Vidarabine)	21704	(2R,3S,4S,5R)-2-(6-aminopurin-9-yl)-5-(hydroxymethyl)oxolane-3,4-diol	Synthetic analog of arabinosyl nucleosides from *Tectitethya crypta*
8.	Phycocyanobilin	365902	3-[2-[[3-(2-carboxyethyl)-5-[(3-ethylidene-4-methyl-5-oxopyrrolidin-2-ylidene)methyl]-4-methyl-1H-pyrrol-2-yl]methylidene]-5-[(4-ethyl-3-methyl-5-oxopyrrol-2-yl) methylidene]-4-methylpyrrol-3-yl]propanoic acid	Phytochrome chromophore extracted from algae (Arthrospira sp.)
9.	Avarol	72185	2-[[(1R,2S,4aS,8aS)-1,2,4a,5-tetramethyl-2,3,4,7,8,8a-hexahydronaphthalen-1-yl] methyl]benzene-1,4-diol	Sponge (*Disidea avara*)
10.	Macrolactin-A	6451096	(3Z,5E,8R,9E,11Z,14S,16S,17E,19E,24R)-8,14,16-trihydroxy-24-methyl-1-oxacyclotetracosa-3,5,9,11,17,19-hexaen-2-one	Marine bacteria
11.	AcDa-1	15954445	[(5R,9R)-1,2-diformyl-5-methyl-8-[(2R)-6-methylhept-5-en-2-yl]-9-bicyclo[3.3.1]non-2-enyl] acetate	Marine algae (*Dictyota menstrualis*)
12.	Esculetin-4-carboxylic acid ethyl ester	11988319	Ethyl 6,7-dihydroxy-2-oxochromene-4-carboxylate	Marine sponge (Axinella cf. corrugate)
13.	Hydroxypentafuhalol A	102274236	5-[4-[6-[2,6-dihydroxy-4-(2,4,6-trihydroxyphenoxy)phenoxy]-2,3,4-trihydroxyphenoxy]-2,6-dihydroxyphenoxy]benzene-1,2,3,4-tetrol	Brown seaweed algae
14.	6,6′-Bieckol	137388	4-(3,5-dihydroxyphenoxy)-9-[6-(3,5-dihydroxyphenoxy)-2,4,7,9-tetrahydroxydibenzo-p-dioxin-1-yl]dibenzo-p-dioxin-1,3,6,8-tetrol	Brown alga (*Ecklonia cava*)

acceptors and log P should not be greater than 5; in which all must be followed or maximum one can be violated for the ligand to be orally active. All of the above compounds which were obeying Lipinski's rule had high GIT absorption with a good bioavailability score of around 0.55 (Table 3). Phycocyanobilin obeyed Lipinski's rule but disobeyed Ghose Rule, Veber, Egan, and Muegge rules. 1-hexadecoxypropane-1,2-diol had conflicting result as it obeys Lipinski and Ghose rule, but didn't agree to Veber and Muegge rule.

3.4. Toxicity prediction

The toxicity prediction gives us a brief idea about the toxic effect that may cause several organs if taken in unwanted doses by analysing the toxicities of the moieties present in the ligand. The toxicity prediction analysis was carried out with the help of eMOLTOX webserver [62]. Among the 14 ligands, only 5 ligands had no toxic activity found in them, rest 10 ligands impart some sort of toxicity. The predicted report revealed that iota-carrageenan, hydroxypentafuhalol-A, and 6,6′-bieckol may cause immunotoxicity by downregulating the effect of TNF-alpha that may decrease apoptosis, cell differentiation, and proliferation. Fostularin 3 can impart toxicities to the heart, blood vessel, kidney, respiratory system by modulating beta-adrenergic receptors at toxic doses. 1-Hexadecoxypropane-1,2-diol have the potential to generate hepatotoxicity as it is cytotoxic to HepG2, HEK293 cells at different time intervals, and antagonistic to Farnesoid-X-receptor (FXR) signalling pathway that may downregulate the effect of hepatocytes. 15 alpha-methoxypuupehenol has seen to cause a maximum grade of toxicities which includes hepatotoxicity, immunotoxicity, genotoxicity and may also affect other organs. Toxic doses of vidarabine function by over-activating p53 signalling pathway which activates apoptosis and activation of H2AX which causes DNA repair. Hydroxypentafuhalol-A, avarol, and 6, 6′-bieckol also cause some sort of hepatotoxicity. The focus must be on modifying these molecules via computer-aided drug design to minimise the toxicities by keeping the potency as it is. The detailed report of predicted toxicities along with the probability of causing the toxicity is given in Table 4.

3.5. Molecular docking of the ligands with Mpro

Till now, there is no approved drug or vaccine available which can effectively inhibit SARS-CoV-2 main protease, hence molecular docking is performed with the pre-existing anti-viral drugs as a trial method to check their efficacy in SARS-CoV-2. The selected 14 compounds were docked at different sites within the generated grid-box of Mpro. This task was carried out at AutoDock 4.2.6 [54]. The macromolecule was selected as a rigid frame name. The number of genetic algorithm runs was kept at 10 and the rest of all the parameters (docking parameters; the maximum number of evals; Autodock 4.2 parameters) were set to default. The file was saved in.DPF format and the result was evaluated using Lamarckian Genetic Algorithm (LGA) (4.2). The 10 different docking conformation results were obtained in.DLG text file. Among the 10 results, the minimum docking score achieved was considered as the final result. The docking scores of all the ligands along with the standard drug (GC376) are represented in Table 5. Among the 14 marine compounds, avarol shows better affinity at the binding site of the receptor with a docking score of −8.05 kcal/mol. The docking results of every ligand were compared with the standard ligand (GC376) and it was seen that five compounds were showing better docking results than the standard drug depicting better affinity with the protein. The docking scores of the best 5 compounds: avarol, AcDa-1, macrolactin-A, 15 alpha-methoxypuupehenol, and phycocyanobilin are −8.05, −7.74, −7.60, −7.15, and −7.11 kcal/mol respectively, whereas the standard drug showed the Gibbs free energy of −6.87 kcal/mol.

After predicting the docking scores, next the protein-ligand

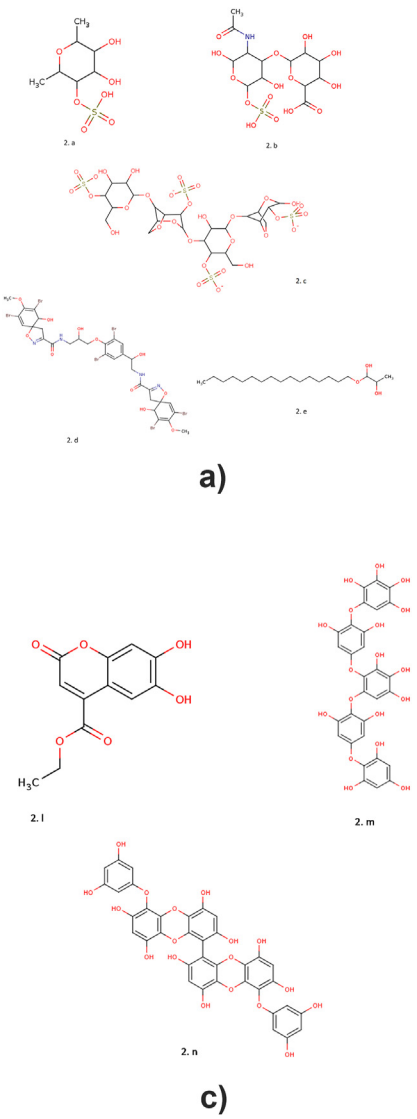

Fig. 1. 2D portrayal of 14 selected natural/semi-synthetic inhibitors of viral replication were selected and their efficacy is to be checked by docking with the main protease of SARS-CoV-2 virus. Compounds: 2.a. Fucoidan, 2.b. Chondroitin sulphate, 2.c. Iota-carrageenan, 2.d. Fostularin 3, 2.e. 1-Hexadecoxypropane-1,2-diol, 2.f. 15 alpha-Methoxypuupehenol, 2.g. Ara- A (Vidarabine), 2.h. Phycocyanobilin, 2.i. Avarol, 2.j. Macrolactin-A, 2.k. AcDa-1, 2.l. Esculetin-4-carboxylic acid ethyl ester, 2.m. Hydroxypentafuhalol A, and 2.n. 6,6′-Bieckol.

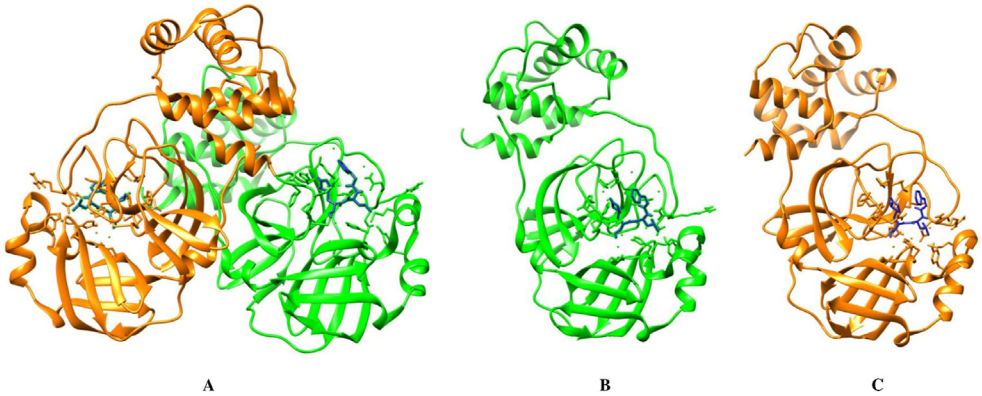

Fig. 2. 3D crystal structure interpretation of Mpro (3CLpro) complexed with GC376 ((1S,2S)-2-({N-[(benzyloxy) carbonyl]-L-leucyl}amino)-1-hydroxy-3-[(3S)-2-oxopyrrolidin-3-yl] propane-1-sulfonic acid)(C21H31N3O8S) (PDB CODE: 7D1M) taken from RCSB PDB. Mpro has 2 subunits (A and B chain). A: Mpro with GC376, B: A chain (depicted in green) with GC376 (depicted in blue), and C: B chain (depicted in orange) with GC376. (For interpretation of the references to colour in this figure legend, the reader is referred to the Web version of this article.)

interactions were analysed to validate whether the ligands are binding with either or both the amino-acids: HIS41 and CYS145 to cause inhibition of the protein [66]. This task was performed at PMV 1.4.6. (Fig. 3). Hydroxypentafuhalol A formed hydrophobic and interactions with the residues THR25, HIS41/172, CYS145, PHE140, LEU141, ASN142, MET165, GLU166, ASP187, GLN189, and hydrogen bonding with amino acids CYS44, SER144, HIS163, and GLN192. Likewise, Fucoidan expressed hydrophobic interactions with PHE140, LEU141, ASN142, SER144, HIS172, and GLU166, while forms 3 H-bonds at position GLY143, CYS145, and HIS163; chondroitin sulphate hydrophobically interlinked with HIS41/164, PHE140, LEU141, ASN142, CYS145, MET165, and GLU166 and forming hydrogen bonding with GLY143, and

Table 2
Predicted physicochemical and pharmacokinetic characteristics of the ligands.

Sl. No.	COMPOUND NAME	MOLECULAR FORMULA	MOL. WT. (gm/mol)	LOG $P_{o/w}$	LOG S	SOLUBILITY	GIT ABSORPTION	BBB PERMEABILITY
1.	Fucoidan	C7H14O7S	242.25	0.47	−0.25	Very soluble	High	No
2.	Chondroitin sulphate	C13H21NO15S	463.37	−1.00	0.75	Highly soluble	Low	No
3.	Iota-carrageenan	C24H34O31S4	946.77	−0.97	1.09	Highly soluble	Low	No
4.	Fostularin 3	C24H34O31S4	1114.01	3.83	−7.07	Poorly soluble	Low	No
5.	1-Hexadecoxypropane-1,2-diol	C19H40O3	316.52	4.22	−5.13	Moderately soluble	High	Yes
6.	15 alpha-Methoxypuupehenol	C22H32O4	360.49	3.40	−5.42	Moderately soluble	High	Yes
7.	Ara- A (Vidarabine)	C10H13N5O4	267.24	0.41	−1.05	Very soluble	Low	No
8.	Phycocyanobilin	C33H38N4O6	586.68	3.25	−4.55	Moderately soluble	Low	No
9.	Avarol	C21H30O2	314.46	3.25	−5.62	Moderately soluble	High	Yes
10.	Macrolactin-A	C24H34O5	402.52	3.42	−5.15	Moderately soluble	High	No
11.	AcDa-1	C22H32O4	360.49	2.95	−4.31	Moderately soluble	High	Yes
12.	Esculetin-4-carboxylic acid ethyl ester	C12H10O6	250.20	1.81	−2.32	Soluble	High	No
13.	Hydroxypentafuhalol A	C30H22O18	670.48	2.57	−5.86	Moderately soluble	Low	No
14.	6,6′-Bieckol	C36H22O18	742.55	2.66	−7.52	Poorly soluble	Low	No

Log $P_{o/w}$: Octanol/water partition coefficient (which determines the lipophilicity of the ligand).
Log S: Solubility in aqueous media.

Table 3
Predicted drug-likeness and oral bioavailability score of the ligands.

SL. NO.	COMPOUND	LIPINSKI RULE	GHOSE RULE	VEBER RULE	EGAN RULE	MUEGGE RULE	BIOAVAILABILITY SCORE
1.	Fucoidan	Yes; 0 violation	Yes	Yes	Yes	Yes	0.56
2.	Chondroitin sulphate	No; 2 violations: N or O>10, NH or OH>5	No	No	No	No	0.11
3.	Iota-carrageenan	No; 3 violations: MW>500, N or O>10, NH or OH>5	No	No	No	No	0.11
4.	Fostularin 3	No; 3 violations: MW>500, N or O>10, NH or OH>5	No	No	No	No	0.17
5.	1-Hexadecoxypropane-1,2-diol	Yes; 0 violation	Yes	No	Yes	No	0.55
6.	15 alpha-Methoxypuupehenol	Yes; 0 violation	Yes	Yes	Yes	No	0.55
7.	Ara- A (Vidarabine)	Yes; 0 violation	No	Yes	No	Yes	0.55
8.	Phycocyanobilin	Yes; 1 violation: MW>500	No	No	No	No	0.11
9.	Avarol	Yes; 1 violation: MLOGP>4.1	Yes	Yes	Yes	No	0.55
10.	Macrolactin-A	Yes; 0 violation	Yes	Yes	Yes	Yes	0.55
11.	AcDa-1	Yes; 0 violation	Yes	Yes	Yes	Yes	0.55
12.	Esculetin-4-carboxylic acid ethyl ester	Yes; 0 violation	Yes	Yes	Yes	Yes	0.55
13.	Hydroxypentafuhalol A	No; 3 violations: MW>500, N or O>10, NH or OH>5	No	No	No	No	0.17
14.	6,6′-Bieckol	No; 3 violations: MW>500, N or O>10, NH or OH>5	No	No	No	No	0.17

HIS163, iota-carrageenan formed hydrophobic interactions with HIS41, MET49/165, ASN142, SER144, CYS145, HIS163, ARG188, GLN189, THR190, and forming 3 H-bonds with HIS163, GLU166, and GLN192, fostularin 3 hydrophobically interacted with THR25/190, HIS41/164, MET49/165, LEU27/141, GLY143, SER144, CYS44/145, GLU166, ASP187, ARG188, and GLN192 with 2 H-bonds with GLN189 and ASN142; 1-hexadecoxypropane-1,2-diol showed pi-pi interactions with HIS41/163, CYS145, MET165, GLU166, ASP187, and ARG188, forming H-bond at THR190, and GLN192, 15 alpha-methoxypuupehenol interacted with HIS41/163, LEU141, ASN142, CYS145, MET165, and GLU166, and interacted via 3 H-bonds ARG188 and GLN192, ara-A forms hydrophobic interaction with PHE140, LEU141, SER144, CYS145, and HIS163/172, and forming 3 H-bonds interactive amino acids with GLY143, ASN142 and GLU166. Phycocyanobilin interacted with THR25/26/190, LEU27, MET49/165, CYS44/145, TYR54, LEU141, ASN142, GLY143, GLU166, ASP187, ARG188, and GLN189/192 with 2 H-bonding at HIS41 and HIS163, avarol presented hydrophobic interactions at HIS41/164, MET49/165, CYS44, ASP187, ARG188, and GLN189 with 5 atoms in hydrogen bonding. Macrolactin-A interrelated at 12 positions THR25, HIS41, MET49/165, LEU141, ASN142, GLY143, SER144, CYS145, GLU166, and ARG188, and forming 2 H-bonds at GLY143 and GLN189, AcDa-1 interacted with hydrophobic interactions at HIS164, CYS44, MET49/165, VAL186, ASP187, ARG188, and GLN192 with 2 H-bonding found at HIS41 and GLU166, esculetin-4-carboxylic acid ethyl ester formed hydrophobic interactions with HIS41, CYS44, MET49/165, TYR54, ASP187, ARG188, GLN192 with 2 H-bonding, and 6,6′-bieckol finally interacted with THR25/26, LEU27, HIS41, ASN142, CYS145, MET165, ASP187, ARG188, and GLN189/192 as well as formed H-bonds interactive amino acids at GLY143. As these findings are predictive, hence need to be validated via MD simulation study. This shows that all the 14 compounds with negative docking scores are showing interactions with either CYS145 or HIS41 or both of them expressing their antagonistic actions. The inhibitory constant (Ki) was also predicted using AutoDock 4.2.6. which confirms their antagonistic action by

Table 4
Predicted toxicities the ligand may have to specific organ of the body.

Sl. No.	COMPOUND NAME	PREDICTED TOXICITY	TARGET	PROBABILITY
1.	Fucoidan	No toxic activity was found in the compound	–	–
2.	Chondroitin sulphate	No toxic activity was found in the compound	–	–
3.	Iota-carrageenan	TNF-alpha modulation	Immune	0.988
4.	Fostularin 3	Beta-1/2/3 adrenergic receptor modulator	Heart, blood vessel, kidney, respiratory system	0.987
		Neuropeptide Y receptor type-1 modulator	GI tract, immune, nervous system	0.988
		Platelet activating factor receptor (PAF) modulator	Immune, respiratory, blood, Heart, Kidney	0.996
5.	1-Hexadecoxypropane-1,2-diol	Cytotoxicity in HepG2 cells - 16 h	Liver	0.993
		Cytotoxicity in HEK293 cells – 8/16/24/32 h	Kidney	0.995
		Cytotoxicity in HepG2 cells - 24 h	Liver	0.981
		Muscarinic acetylcholine receptor (M4) modulator	Brain, Heart	0.988
		Farnesoid-X-receptor (FXR) signaling pathway antagonist	Liver	0.982
6.	15 alpha-Methoxypuupehenol	Androgen receptor (AR) signaling pathway agonist	Central nervous system, Endocrine system	0.985
		Retinoic acid receptor (RAR) signaling pathway antagonist	Immune system	0.995
		Heat shock response signaling pathway activator	Liver	0.991
		Farnesoid-X-receptor (FXR) signaling pathway antagonist	Liver	0.992
		Glucocorticoid receptor modulator	Endocrine, immune, Nervous system	0.986
		Dopamine D1 receptor modulator	Central nervous system, Kidney, Heart	0.997
		Thyroid stimulating hormone receptor (TSHR) signaling pathway agonist	Endocrine, Heart	0.987
		Cannabinoid CB1 receptor modulator	Nervous system, Heart	0.985
		Differential cytotoxicity against isogenic chicken DT40 cell lines with known DNA damage response pathways - Rad54/Ku70 mutant cell line	Genotoxicity	0.993
		Retinoid-related orphan receptor gamma (ROR-gamma) signaling pathway antagonist	Immune	0.987
7.	Ara- A (Vidarabine)	A3- adenosine receptor	Nervous system, respiratory	0.996
		Antagonist of the constitutive androstane receptor (CAR) signaling pathway	Liver	0.995
		Agonist of the p53 signaling pathway	Tumor suppression	0.995
		Agonist of the RXR signaling pathway	Liver	0.99
		Agonist of H2AX	DNA damage	0.996
8.	Phycocyanobilin	No toxic activity was found in the compound	–	–
9.	Avarol	Estrogen receptor alpha (ER-alpha) agonist	Endocrine	0.992
		Retinoic acid receptor (RAR) antagonist	Immune	0.986
		Thyroid receptor (TR) signaling pathway antagonist	Endocrine, Heart	0.996
		Antagonist of the constitutive androstane receptor (CAR) signaling pathway	Liver	0.989
		Farnesoid-X-receptor (FXR) signaling pathway antagonist	Liver	0.996
		Cytotoxicity in HepG2 cells - 32 h	Liver	0.994
		Differential cytotoxicity (isogenic chicken DT40 cell lines)	Genotoxicity	0.989
				0.989

(continued on next page)

Table 4 (*continued*)

Sl. No.	COMPOUND NAME	PREDICTED TOXICITY	TARGET	PROBABILITY
		Modulator of Dopamine D1 receptor	Central nervous system, Kidney, Heart	
		Glucocorticoid receptor modulator	Endocrine, immune, Nervous system	0.987
10.	Macrolactin-A	No toxic activity was found in the compound	–	–
11.	AcDa-1	Glucocorticoid receptor (GR) antagonist	Endocrine, immune, Nervous system	0.986
		Differential cytotoxicity against isogenic chicken DT40 cell lines with known DNA damage response pathways - Rad54/Ku70 mutant cell line	Genotoxicity	0.98
		Muscarinic acetylcholine receptor- M4 modulator	Nervous system, Heart	0.984
12.	Esculetin-4-carboxylic acid ethyl ester	No toxic activity was found in the compound	–	–
13.	Hydroxypentafuhalol-A	Agonist of Liver X receptor alpha	Liver	0.992
		TNF-alpha receptor modulator	Immune	0.99
14.	6,6′-Bieckol	Agonist of Liver X receptor alpha	Liver	0.992
		Modulator of TNF-alpha	Immune	0.987

Table 5
Table depicting the docking scores of the 14 compounds obtained from marine sources. The docking was evaluated using Lamarckian Genetic Algorithm where 10 different docking conformations were acquired. Among them, the conformation which gave the lowest binding free energy was considered as the docking score. The docking score was compared with standard ligand (GC376).

Sl. No.	COMPOUND NAME	BEST RUN ΔG value (kcal/mol) USING AUTODOCK 4.2.6	PREDICTED Ki OF BEST RUN AT 298.15 K (μM)
1.	Fucoidan	−3.66	2080
2.	Chondroitin sulphate	−4.51	496.56
3.	Iota-carrageenan	−0.18	740360
4.	Fostularin 3	−2.03	32240
5.	1-Hexadecoxypropane-1,2-diol (21646261)	−3.27	3980
6.	15 alpha-Methoxypuupehenol (21591485)	−7.15	5.70
7.	Ara- A (Vidarabine)	−5.08	189.00
8.	Phycocyanobilin	−7.11	6.12
9.	**Avarol**	**−8.05**	**1.26**
10.	Macrolactin-A	−7.60	2.69
11.	**AcDa-1**	**−7.74**	**2.12**
12.	Esculetin-4-carboxylic acid ethyl ester	−5.44	102.36
13.	Hydroxypentafuhalol A	−3.06	5670
14.	6,6′-Bieckol	−2.40	17400
15.	GC376 (STANDARD)	−6.87	9.15

predicting the potency of the inhibitor. Simply, Ki refers to the amount of drug required which causes half of the maximum inhibition. It is also depicted as IC50. The lesser the Ki value, the more potent is the drug. Here, the top 5 compounds with the best potency are the compounds that have the best docking scores which include avarol, AcDa-1, macrolactin-A, 15 alpha-methoxypuupehenol, and phycocyanobilin with a Ki of 1.26, 2.12, 2.69, 5.70, and 6.12 μM respectively.

3.6. MD simulation study

Since molecular docking studies were done using the rigid crystal structure of SARS-CoV-2 Mpro, we have evaluated target receptor and lead compounds interactions in the dynamic behaviour of both receptor and ligand using molecular dynamic simulation to obtain the stable binding conformation and further validate the docking result of lead compounds within the cavity of SARS-CoV-2 Mpro. As observed from Table 5, Avarol and AcDa-1 were found to have docking scores higher than among screened compounds. Hence, Avarol and AcDa-1 in complex with SARS-CoV-2 Mpro were carried out molecular dynamic simulation for 100 ns, using simple point charge (SPC) water mode. The Root Mean Square Deviation (RMSD), Root Mean Square Fluctuation (RMSF), and Protein-Ligand Contacts were analysed from the MD simulation trajectories to reveal thermodynamic conformational stability during 100 ns period. Analysis of MD simulation trajectories through RMSD parameters can provide stability of the protein backbone when bound with the specific ligand within the dynamic condition. It also provides brief insights into its structural conformation during the MD simulation. It is implicated that as minor as the RMSD value throughout the MD simulated trajectory suggests higher stability of the protein-ligand complex, whereas higher RMSD value shows comparatively low stability of the protein-ligand complex [59].

The RMSD graph result of Avarol is shown in Fig. 4A. Initially, the graph line showed little stability from 2 to 57 ns having RMSD value range from 1.2 to 2.0 Å; after that slight fluctuation at 57 ns, a promising result was observed. The graph line is stable until 100ns having a constant RMSD value 3.2 Å. RMSD plot of AcDa-1 shows that initially constant trend were observed from 1ns to 54ns with RMSD ~2 Å, later little fluctuation at 54 ns, constant graph were observed until 100 ns with RMSD value of 2.4 Å (Fig. 4B). The overall RMSD analysis revealed that fluctuations in a graph in the whole simulation were within the standard range of RMSD 1–3 Å which indicates that the reported lead compound bound tightly within the cavity of SARS- CoV-2 Mpro enzyme binding pocket.

The RMSF plot represents the mobility and flexibility of each protein residue throughout the simulation. Higher RMSF values indicate higher flexibility during the MD simulation while the lower value of RMSF reflects the good stability of the system [59]. In this plot, the protein residues that contacts with the ligand are represented with vertical green lines, Secondary structural elements such as alpha-helical and beta-strand regions are displayed in red and blue backgrounds, respectively, while white background indicates loop region. Alpha helices and beta strands typically are rigid than the unstructured part of the protein and thus fluctuate less than the loop regions. High fluctuations were observed in N- and C terminal region compared to any other part of the protein. If the fluctuation of the active site and the main chain atoms was mild, it indicated that the conformational change was slight. The RMSF plot of avarol (Fig. 5A) and AcDa-1(Fig. 5B) with SARS-CoV-2 Mpro complex yielded little fluctuations with less than 3 Å at ligand contacted residues which is perfectly acceptable for small globular proteins.

Furthermore, protein interaction with the ligand is monitored throughout the simulation, these interactions are categorised into: hydrogen bonds, hydrophobic, and water bridges as shown in Fig. 6. Hydrogen bond interaction plays an imperative role due to strong bond formation in ligand binding. For Avarol-SARS-CoV-2 Mpro complex hydrogen bond interaction is seen with HIS41, CYS44, SER46, HIS163, GLU166, GLN192, and ALA193. Water bridges with these residues were

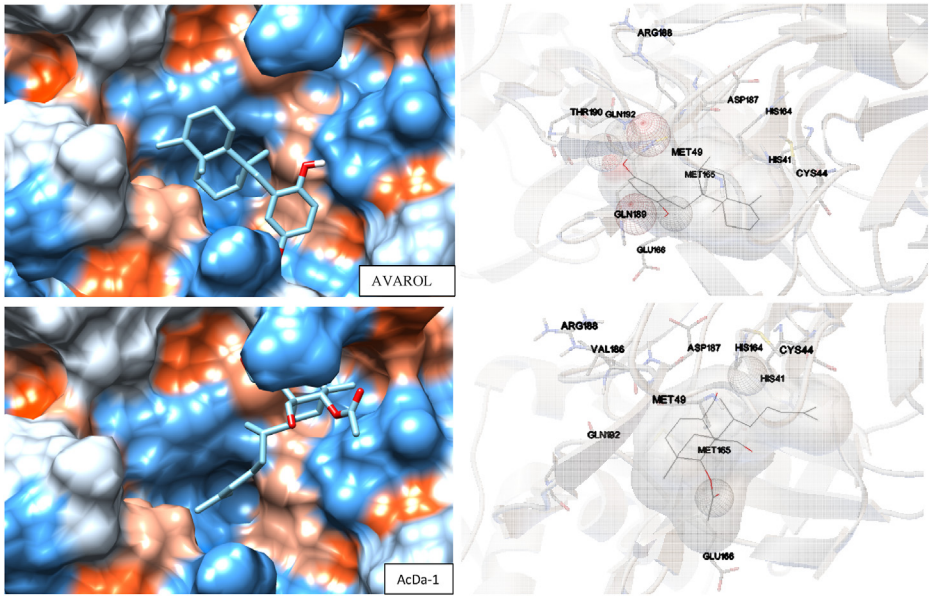

Fig. 3. The left side illustration depicts the docking conformation of Avarol and AcDa-1 at the hydrophobic active binding surface of Mpro enzyme of SARS-CoV-2 virus, and the right portion describes the interactions of ligands with specific amino acids of the protein at the binding site along with the predicted H-bonds formed portrayed in sphere.

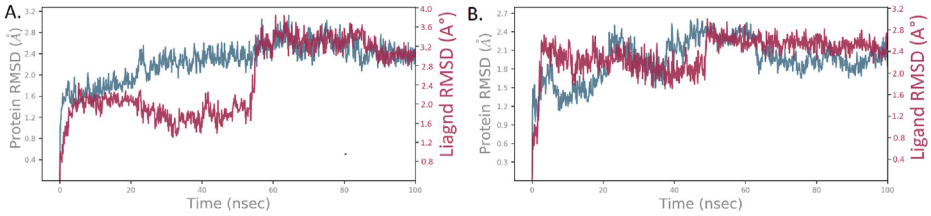

Fig. 4. Time-dependent Protein-ligand RMSD plot (Angstrom) of the **A.** Avarol, **B.** AcDa-1 with SARS-CoV-2 Mpro enzyme binding pocket.

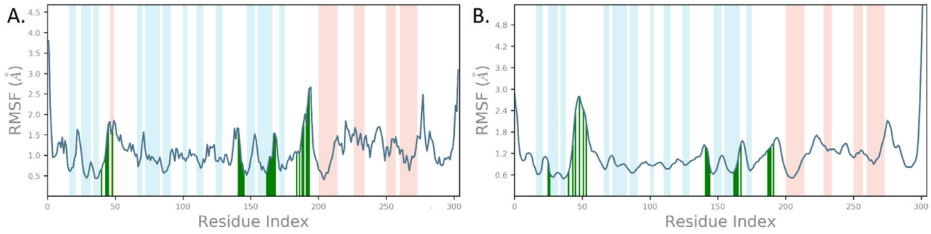

Fig. 5. Time-dependent Protein RMSF plot (Angstrom) of the **A.** Avarol, **B**. AcDa-1 with SARS-CoV-2 Mpro enzyme binding pocket.

also found as key interaction bonds. Also, Major hydrophobic interactions were seen with HIS41, MET49, MET165, and PRO168. Importantly, π- π interactions with catalytic dyad HIS41 residue were also seen at an average of 10% (Fig. 6A). For AcDa-1-SARS-CoV-2 Mpro complex hydrogen bond interaction is seen with HIS41, ASN142, CYS145, GLU66, and GLN189. while, LEU27, MET49, PRO52, and MET165 amino acid residues show hydrophobic interactions (Fig. 6B).

4. Conclusion and future perspectives

Marine compounds have an immense potential to treat numerous pathologies, but the majority of them still remain unexplored. In this experiment, we screened 14 natural/semisynthetic compounds: fucoidan, chondroitin sulphate, iota-carrageenan, fostularin 3, 1-hexadecoxypropane-1,2-diol, 15 alpha-methoxypuupehenol, ara- A (vidarabine), phycocyanobilin, avarol, macrolactin-A, AcDa-1, esculetin-4-carboxylic acid ethyl ester, hydroxypentafuhalol A, and 6,6′-bieckol, and targeted them against the main protease enzyme, Mpro (PDB ID: 7D1M) of the virus in order to inhibit it using computational modelling. Among these 14 selected compounds, avarol yields the best docking score of −8.05 kcal/mol. All the 14 compounds were seen to form interactions with at least one of the 2 catalytic regions (CYS145 and HIS41) of Mpro. Out of these 5 best scores, macrolactin-A, 15 alpha-methoxypuupehenol, and phycocyanobilin bind with both the catalytic regions. The inhibitory activity of avarol and AcDa-1 were several times more than the known peptide-based inhibitor.

The protein-ligand interactions and their respective hydrogen bonding obtained from docking were validated using molecular dynamics simulation study. The MD simulation was carried out for 100 ns using Schrödinger Desmond tool to predict the thermodynamic stability and binding conformations by analysing the RMSD and RMSF plots for the protein-ligand complex [57]. Equilibrium conditions were achieved

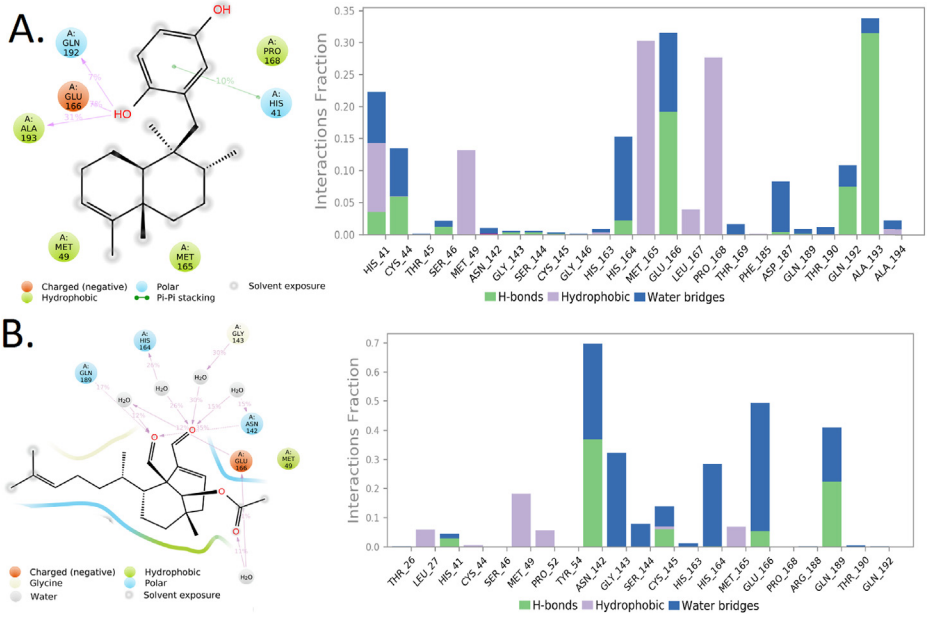

Fig. 6. Simulation Interactions Diagram, 2D binding interaction of **A.** Avarol, **B.** AcDa-1 with SARS-CoV-2 Mpro enzyme binding pocket along with bar diagram.

in both ligands after a specific period of time in RMSD vs time plot, and the fluctuations in a graph in the whole simulation were within the standard range of RMSD 1–3 Å, thus confirming better conformational dynamics of the complex. ADME analysis revealed Avarol imparts moderate water solubility with high GIT permeability. Moreover, it was obeying Lipinski, Ghose, Weber, and Evan's rule with an oral bioavailability score of 0.55. All of these make it feasible for oral absorption. In spite of moderate docking results, 5 compounds: fucoidan, chondroitin sulphate, phycocyanobilin, macrolactin-A, and esculetin-4-carboxylic acid ethyl ester didn't exhibit any serious toxic effects which signify better safety of these drugs with a wide therapeutic index. Avarol may impart some sort of hepatotoxicity, genotoxicity, and immunotoxicity at toxic doses. Further, more diverse research is required as these are just the predicted results. More piece of in-vitro and in-vivo studies are needed to be carried out to potentially target SARS-CoV-2 and contain this COVID-19 pandemic.

Funding statement

This research did not receive any specific grant from funding agencies in the public, commercial, or not-for-profit sectors.

Declaration of competing interest

The authors declare that they have no known competing financial interests or personal relationships that could have appeared to influence the work reported in this paper.

References

[1] Mackenzie John S, Smith David W. COVID-19: a novel zoonotic disease caused by a coronavirus from China: what we know and what we don't. Microbiol. Australia Mar. 2020;17. https://doi.org/10.1071/MA20013. MA20013.
[2] Pal Mahendra, et al. Severe acute respiratory syndrome coronavirus-2 (SARS-CoV-2): an update. Cureus 26 Mar. 2020;12:3. https://doi.org/10.7759/cureus.7423. e7423.
[3] Singhal Tanu. A review of coronavirus disease-2019 (COVID-19). Indian J. Pediatr. 2020;87(4):281–6. https://doi.org/10.1007/s12098-020-03263-6.
[4] Kumar Purnima, et al. The nonstructural protein 8 (nsp8) of the SARS coronavirus interacts with its ORF6 accessory protein. Virology 2007;366(2):293–303. https://doi.org/10.1016/j.virol.2007.04.029.
[5] Naqvi Ahmad Abu Turab, et al. Insights into SARS-CoV-2 genome, structure, evolution, pathogenesis and therapies: structural genomics approach. Biochim. Biophys. Acta (BBA) - Mol. Basis Dis. 2020;1866(10):165878. https://doi.org/10.1016/j.bbadis.2020.165878.
[6] Mousavizadeh Leila, Ghasemi Sorayya. Genotype and phenotype of COVID-19: their roles in pathogenesis. J. Microbiol. Immunol. Infect. = Wei mian yu gan ran za zhi 2020;31. https://doi.org/10.1016/j.jmii.2020.03.022. Mar.
[7] Elmezayen Ammar D, et al. Drug repurposing for coronavirus (COVID-19): in silico screening of known drugs against coronavirus 3CL hydrolase and protease enzymes. J. Biomol. Struct. Dynam. 26 Apr. 2020:1–13. https://doi.org/10.1080/07391102.2020.1758791.
[8] Bhatia Rohit, et al. Strategies and challenges to develop therapeutic candidates against COVID-19 pandemic. Open Virol. J. 2020;14(1):16–21. https://doi.org/10.2174/1874357902014010016.
[9] Yasuhara-Bell Jarred, Lu Yuanan. Marine compounds and their antiviral activities. Antivir. Res. 2010;86(3):231–40. https://doi.org/10.1016/j.antiviral.2010.03.009.
[10] Ye, Zi-Wei et al. "Zoonotic origins of human coronaviruses." Int. J. Biol. Sci. vol. 16,10 1686-1697. 15 Mar. 2020, doi:10.7150/ijbs.45472.
[11] Conzade Romy, et al. Reported direct and indirect contact with dromedary camels among laboratory-confirmed MERS-CoV cases. Viruses 2018;10:8–425. https://doi.org/10.3390/v10080425. 13 Aug.
[12] Frutos Roger, et al. COVID-19: time to exonerate the pangolin from the transmission of SARS-CoV-2 to humans. Infect. Genet. Evol. 2020;84:104493. https://doi.org/10.1016/j.meegid.2020.104493.
[13] Liu Ying, et al. The reproductive number of COVID-19 is higher compared to SARS coronavirus. J. Trav. Med. 2020;27(2). https://doi.org/10.1093/jtm/taaa021. taaa021.
[14] Li Qun, et al. Early transmission dynamics in Wuhan, China, of novel coronavirus-infected pneumonia. N. Engl. J. Med. 2020;382(13):1199–207. https://doi.org/10.1056/NEJMoa2001316.
[15] Malki Zohair, et al. ARIMA models for predicting the end of COVID-19 pandemic and the risk of second rebound. Neural Comput. Appl. 2020. https://doi.org/10.1007/s00521-020-05434-0.
[16] Bajgain Kalpana Thapa, et al. Prevalence of comorbidities among individuals with COVID-19: a rapid review of current literature. Am. J. Infect. Control 2020;S0196–6553(20):30637–44. https://doi.org/10.1016/j.ajic.2020.06.213. 10 Jul.
[17] Lauer Stephen A, et al. The incubation period of coronavirus disease 2019 (COVID-19) from publicly reported confirmed cases: estimation and application. Ann. Intern. Med. 2020;172(9):577–82. https://doi.org/10.7326/M20-0504.
[18] Tang Tiffany, et al. Coronavirus membrane fusion mechanism offers a potential target for antiviral development. Antivir. Res. 2020;178:104792. https://doi.org/10.1016/j.antiviral.2020.104792.
[19] Prajapat Manisha, et al. Drug targets for corona virus: a systematic review. Indian J. Pharmacol. 2020;52(1):56–65. https://doi.org/10.4103/ijp.IJP_115_20.
[20] McBride Ruth, et al. The coronavirus nucleocapsid is a multifunctional protein. Viruses 7 Aug. 2014;6:8 2991–3018. https://doi.org/10.3390/v6082991.
[21] Masters Paul S. The molecular biology of coronaviruses. Adv. Virus Res. 2006;66:193–292. https://doi.org/10.1016/S0065-3527(06)66005-3.
[22] Huang Yuan, et al. Structural and functional properties of SARS-CoV-2 spike protein: potential antivirus drug development for COVID-19. Acta Pharmacol. Sin. 2020;41(9):1141–9. https://doi.org/10.1038/s41401-020-0485-4.
[23] Bertram Stephanie, et al. Cleavage and activation of the severe acute respiratory syndrome coronavirus spike protein by human airway trypsin-like protease. J. Virol. 2011;85(24):13363–72. https://doi.org/10.1128/JVI.05300-11.

[24] Báez-Santos Yahira M, et al. The SARS-coronavirus papain-like protease: structure, function and inhibition by designed antiviral compounds. Antivir. Res. 2015;115: 21–38. https://doi.org/10.1016/j.antiviral.2014.12.015.
[25] Sicari Daria, et al. Role of the early secretory pathway in SARS-CoV-2 infection. JCB (J. Cell Biol.) 2020;219(9). https://doi.org/10.1083/jcb.202006005.
[26] Anand Kanchan, et al. Coronavirus main proteinase (3CLpro) structure: basis for design of anti-SARS drugs. Science 2003;300(5626):1763–7. https://doi.org/10.1126/science.1085658.
[27] McKee Dwight L, et al. Candidate drugs against SARS-CoV-2 and COVID-19. Pharmacol. Res. 2020;157:104859. https://doi.org/10.1016/j.phrs.2020.104859.
[28] Chen Yu Wai, et al. Prediction of the SARS-CoV-2 (2019-nCoV) 3C-like protease (3CL ^{pro}) structure: virtual screening reveals velpatasvir, ledipasvir, and other drug repurposing candidates. F1000Research 21 Feb. 2020;9 129. https://doi.org/10.12688/f1000research.22457.2.
[29] Teli Divya M, et al. In silico screening of natural compounds as potential inhibitors of SARS-CoV-2 main protease and spike RBD: targets for COVID-19. Front. Mol. Biosci. 19 Jan. 2021;7 599079. https://doi.org/10.3389/fmolb.2020.599079.
[30] Ibrahim Mahmoud AA, et al. In-silico drug repurposing and molecular dynamics puzzled out potential SARS-CoV-2 main protease inhibitors. J. Biomol. Struct. Dynam. 2021;39(15):5756–67. https://doi.org/10.1080/07391102.2020.1791958.
[31] Barré J, Sabatier J-M, Annweiler C. Montelukast drug may improve COVID-19 prognosis: a review of evidence. Front. Pharmacol. 2020;11.
[32] Cortese Marianna, et al. Timing of use of cod liver oil, a vitamin D source, and multiple sclerosis risk: the EnvIMS study. Mult. Scler. 2015;21(14):1856–64. https://doi.org/10.1177/1352458515578770.
[33] Li Bo, et al. Fucoidan: structure and bioactivity. Molecules 12 Aug. 2008;13(8): 1671–95. https://doi.org/10.3390/molecules13081671.
[34] Atashrazm, Farzaneh et al. "Fucoidan and cancer: a multifunctional molecule with anti-tumor potential." Mar. Drugs vol. 13,4 2327-2346. 14 Apr. 2015, doi:10.3390/md13042327.
[35] Lin Yuan, et al. The anti-cancer effects of fucoidan: a review of both in vivo and in vitro investigations. Cancer Cell Int. 7 May. 2020;20 154. https://doi.org/10.1186/s12935-020-01233-8.
[36] Sano Yoh. Antiviral activity of chondroitin sulphate against infection by Tobacco mosaic virus. Carbohydr. Polym. 1997;33(2–3):125–9. https://doi.org/10.1016/s0144-8617(97)00029-5.
[37] Cunha Ludmylla, Grenha Ana. Sulphated seaweed polysaccharides as multifunctional materials in drug delivery applications. Mar. Drugs 25 Feb. 2016; 14(3):42. https://doi.org/10.3390/md14030042.
[38] Gerber P, et al. Protective effect of seaweed extracts for chicken embryos infected with influenza B or mumps virus. In: Proceedings of the Society for Experimental Biology and Medicine. Society for Experimental Biology and Medicine (New York, N.Y.). vol. 99; 1958. p. 590–3. https://doi.org/10.3181/00379727-99-24429. 3.
[39] Nasu Stephanie S, et al. Puupehenone-related metabolites from two Hawaiian sponges, Hyrtios Spp. J. Organ. Chem. 1995;60(22):7290–2. https://doi.org/10.1021/jo00127a039.
[40] Anjum Komal, et al. Marine sponges as a drug treasure. Biomol. Therapeut. 2016; 24(4):347–62. https://doi.org/10.4062/biomolther.2016.067.
[41] Chen Yi-Hsiang, et al. Well-tolerated Spirulina extract inhibits influenza virus replication and reduces virus-induced mortality. Sci. Rep. 2016;6:24253. https://doi.org/10.1038/srep24253. 12 Apr.
[42] Batke E, et al. Action of the antileukemic and anti-HTLV-III (anti-HIV) agent avarol on the levels of superoxide dismutases and glutathione peroxidase activities in L5178y mouse lymphoma cells. Cell Biochem. Funct. 1988;6(2):123–9. https://doi.org/10.1002/cbf.290060207.
[43] Yuan Jun, et al. Antibacterial compounds-macrolactin alters the soil bacterial community and abundance of the gene encoding PKS. Front. Microbiol. 29 Nov. 2016;7(1904). https://doi.org/10.3389/fmicb.2016.01904.
[44] Pereira HS, et al. Antiviral activity of diterpenes isolated from the Brazilian marine alga Dictyota menstrualis against human immunodeficiency virus type 1 (HIV-1). Antivir. Res. 2004;64(1):69–76. https://doi.org/10.1016/j.antiviral.2004.06.006.
[45] Lira Simone P, et al. A SARS-coronovirus 3CL protease inhibitor isolated from the marine sponge Axinella Cf. Corrugata: structure elucidation and synthesis. J. Braz. Chem. Soc. 2007;18(2):440–3. https://doi.org/10.1590/s0103-50532007000200030.
[46] Hamill Pamela, et al. Development of a red-shifted fluorescence-based assay for SARS-coronavirus 3CL protease: identification of a novel class of anti-SARS agents from the tropical marine sponge Axinella corrugata. Biol. Chem. 2006;387(8): 1063–74. https://doi.org/10.1515/BC.2006.131.
[47] Gentile Davide, et al. Putative inhibitors of SARS-CoV-2 main protease from A library of marine natural products: a virtual screening and molecular modeling study. Mar. Drugs 2020;18:4–225. https://doi.org/10.3390/md18040225. 23 Apr.
[48] Artan Murat, et al. Anti-HIV-1 activity of phloroglucinol derivative, 6,6'-bieckol, from Ecklonia cava. Bioorg. Med. Chem. 2008;16(17):7921–6. https://doi.org/10.1016/j.bmc.2008.07.078.
[49] Kim Eb, Kwak Jh. Antiviral phlorotannin from Eisenia bicyclis against human papilloma virus in vitro. Planta Med. 2015;81. https://doi.org/10.1055/s-0035-1565646. 16.
[50] Kim Sunghwan, et al. PubChem 2019 update: improved access to chemical data. Nucleic Acids Res. 2019;47(D1):D1102–9. https://doi.org/10.1093/nar/gky1033.
[51] Wishart David S, et al. DrugBank: a comprehensive resource for in silico drug discovery and exploration. Nucleic Acids Res. 2006;34:D668–72. https://doi.org/10.1093/nar/gkj067. Database issue.
[52] Berman HM, et al. The protein data bank. Nucleic Acids Res. 2000;28(1):235–42. https://doi.org/10.1093/nar/28.1.235.
[53] Pettersen Eric F, et al. UCSF Chimera–a visualization system for exploratory research and analysis. J. Comput. Chem. 2004;25(13):1605–12. https://doi.org/10.1002/jcc.20084.
[54] Morris Garrett M, et al. AutoDock4 and AutoDockTools4: automated docking with selective receptor flexibility. J. Comput. Chem. 2009;30(16):2785–91. https://doi.org/10.1002/jcc.21256.
[55] Sanner MF. Python: a programming language for software integration and development. J. Mol. Graph. Model. 1999;17(1):57–61.
[56] The PyMOL Molecular Graphics System, Version 2.4.1 Schrödinger, LLC.
[57] Shaw DE. Desmond Molecular Dynamics System. New York, NY: Maestro-Desmond Interoperability Tools, Schrödinger; 2018. Research, New York, NY, 2018-4.
[58] Patel Harun M, et al. In silico search of triple mutant T790M/C797S allosteric inhibitors to conquer acquired resistance problem in non-small cell lung cancer (NSCLC): a combined approach of structure-based virtual screening and molecular dynamics simulation. J. Biomol. Struct. Dynam. 2020:1–15. https://doi.org/10.1080/07391102.2020.1734092. 6 Mar.
[59] Ahmad Iqrar, et al. p38α MAP kinase inhibitors to overcome EGFR tertiary C797S point mutation associated with osimertinib in non-small cell lung cancer (NSCLC): emergence of fourth-generation EGFR inhibitor. J. Biomol. Struct. Dynam. 2020: 1–14. https://doi.org/10.1080/07391102.2020.1844801. 11 Nov.
[60] Daina Antoine, et al. SwissADME: a free web tool to evaluate pharmacokinetics, drug-likeness and medicinal chemistry friendliness of small molecules. Sci. Rep. 2017;7:42717. https://doi.org/10.1038/srep42717. 3 Mar.
[61] Dong Jie, et al. ADMETlab: a platform for systematic ADMET evaluation based on a comprehensively collected ADMET database. J. Cheminf. 26 Jun. 2018;10(29):1. https://doi.org/10.1186/s13321-018-0283-x.
[62] Ji Changge, et al. eMolTox: prediction of molecular toxicity with confidence. Bioinformatics 2018;34(14):2508–9. https://doi.org/10.1093/bioinformatics/bty135.
[63] ACD/ChemSketch, version 2018.2.5. Toronto, ON, Canada: Advanced Chemistry Development, Inc.; 2018. www.acdlabs.com.
[64] Gioia Magda, et al. Role of proteolytic enzymes in the COVID-19 infection and promising therapeutic approaches. Biochem. Pharmacol. 2020;182:114225. https://doi.org/10.1016/j.bcp.2020.114225.
[65] Kneller Daniel W, et al. Structural plasticity of SARS-CoV-2 3CL M^{pro} active site cavity revealed by room temperature X-ray crystallography. Nat. Commun. 24 Jun. 2020;11:1–3202. https://doi.org/10.1038/s41467-020-16954-7.
[66] Al-Zaqri, Nabil, et al. Structural and physico-chemical evaluation of melatonin and its solution-state excited properties, with emphasis on its binding with novel coronavirus proteins. J. Mol. Liq. 2020;318:114082. https://doi.org/10.1016/j.molliq.2020.114082.